Pergamon

Int. J. Solids Structures Vol. 32, No. 14, pp. 2009–2021, 1995
Elsevier Science Ltd
Printed in Great Britain
0020–7683/95 $9.50 + .00

0020–7683(94)00228–2

DYNAMIC PLASTIC RESPONSE OF THIN CIRCULAR PLATES STRUCK TRANSVERSELY BY NONBLUNT MASSES

WEI QIN SHEN
Department of Mechanical and Manufacturing Engineering, The University of Portsmouth, Portsmouth, Hants PO1 3DJ, U.K.

(*Received* 24 *January* 1994; *in revised form* 31 *August* 1994)

Abstract—A theoretical analysis is presented which examines the dynamic plastic response of thin circular plates struck transversely by a mass with a conical head and a spherical nose at the centre of the plates. The analysis employs an interaction yield surface which combines the bending moment and membrane force required for plastic flow. Material strain rate sensitive effects are considered with the aid of the Cowper–Symonds equation and Perrone and Bhadra's approximation. Good agreement between the theoretical predictions and the experimental results has been obtained on the maximum permanent deflections and the maximum forces between striker and plates for various impact energies.

NOMENCLATURE

D	material constant in eqn (3b)
E_i	plastic work due to local indentation
E_{if}	plastic work associated with permanent local indentation
E_k	imput kinetic energy
F_1, F_2, F_3	functions defined in eqns (45a–c)
G	mass of a striker
H	plate thickness
K	strengthening factor due to strain rate effect
L	half length of beam
M	bending moment during phase I
M_{do}	dynamic fully plastic bending moment
M_r, M_θ	radial and circumferential bending moments, respectively
M^*, M_r^*, M_θ^*	M/M_{do}, M_r/M_{do} and M_θ/M_{do}, respectively
N	membrane force
N_{do}	dynamic fully plastic membrane force
N_r, N_θ	radial and circumferential membrane forces, respectively
N^*, N_r^*, N_θ^*	N/N_{do}, N_r/N_{do} and N_θ/N_{do}, respectively
P	impact force between striker and plate
P_{max}	maximum impact force occurring when motion ceases
P^*	$P/(2\pi M_{do})$
Q	transverse shear force
Q_{do}	dynamic fully plastic transverse shear force
Q^*	Q/Q_{do}
R	radius of plate
S	side length of square plate
V	part of initial velocity of striker that produces only global deformation
V_o	initial velocity of striker
V_o^*	V_o/H
W	maximum global deflection
W_1	maximum global deflection at the end of phase I
W_f	maximum permanent global deflection
W_i	maximum local indentation
W_{if}	maximum permanent local indentation
W_t	maximum total deflection
W_{tf}	maximum permanent total deflection
W^*	W/H
a	radius of sphere on the head of striker, as shown in Fig. 5
a^*	a/H
f	function presented in eqn (8)

© Crown copyright (1995).

f', f''	df/dr^* and d^2f/dr^{*2}, respectively
p	material constant in eqn (3b)
r	radial coordinate
r^*	r/H
t	time
t_1	time at the end of phase 1
t_f	time when motion ceases
$\dot{w}$	global transverse velocity field defined in eqns (18a,b)
z	coordinate along axial axis
z^*	z/H
Γ	function defined in eqns (30a,b)
$\dot{\Delta}$	increment of radial elongation
Ψ, Ψ_1	functions defined in eqns (29) and (33), respectively
β	$3\sigma_o/(\rho R^2)$
δ	$G/(\rho\pi R^2 H)$
ε_r	radial membrane strain
$\dot{\varepsilon}_m$	mean strain rate
ζ	radius of local indentation in the r direction in Fig. 2
ζ_f	maximum ζ when motion ceases
ζ^*	ζ/H
ζ_δ^*	defined as in eqn (43c)
η	radius of curvature of local indentation in θ direction in Fig. 2
η^*	η/H
θ	circumferential coordinate
κ_r, κ_θ	generalized radial and circumferential bending strains, respectively
λ	$2\varepsilon_r/(H\kappa_r)$
ν	γ/δ
ξ	location of a travelling plastic hinge
ξ^*	ξ/R
ρ	density of material
σ_{do}	dynamic yield stress
σ_o	static yield stress in a uniaxial tensile specimen
$\dot{(\ )}$	$\partial(\ )/\partial t$
$\ddot{(\ )}$	$\partial^2(\ )/\partial t^2$

1. INTRODUCTION

The dynamic plastic responses of thin circular plates struck transversely by nonblunt masses have been examined by several authors. Hopkins (1953) treated this problem with a specified motion of projectile *a priori* and no dynamic interaction between projectile and plate was considered. Kelly and Wierzbicki (1967), Kelly and Wilshaw (1968) and Calder *et al.* (1971) considered the interaction of the striker and the plates with a bending-only method. The assumption of a projectile having a negligible radius is used in Kelly and Wierzbicki (1967) and the plates studied in Calder *et al.* (1971) were assumed to have infinite diameter. Kelly and Wilshaw (1968) presented their experimental results on clamped circular steel plates ($H/2R = 0.05$) struck normally by cylindrical projectiles at speeds of 92–594 m s^{-1}. The maximum displacements in the Kelly–Wilshaw tests were only of the same order as the plate thickness and no penetrations were investigated. Goldsmith *et al.* (1965) published their experimental results on freely suspended thin square aluminum plates ($H/S = 0.001$ and 0.0026) and clamped circular thin plates ($H/2R = 0.00357$) struck elastically by cylindrical projectiles at velocities ranging from 3–22 m s^{-1} and elasto-plastically by cylindro-conical projectiles at velocities ranging from 79–116 m s^{-1}. Results both with and without perforation were investigated in Goldsmith *et al.* (1965) and petalling failures were found on the plates penetrated by cylindro-conical projectiles. Calder and Goldsmith (1971) presented their experimental results on clamped aluminum and steel plates ($H/2R = 0.0035$) and freely suspended square aluminum plates ($H/S = 0.001$) struck transversely by spherical or cylindro-conical steel projectiles at velocities ranging from 23 to 167 m s^{-1}. Results both with and without perforation were investigated by Calder and Goldsmith (1971), who employed an energy approach and membrane-only assumption with an assumed permanent deflection to predict the responses of the plates. Two failure modes of plug and petalling which are associated with the spherical and cylindro-conical projectiles, respectively, were found by Calder and Goldsmith (1971). The variations of velocity drop against the impact velocity were plotted in Figs 22 and 23 in Calder and Goldsmith (1971) for comparison of

experimental results with the theoretical predictions using a formula proposed by Recht and Ipson (1963) with two associated ballistic limits.

The theoretical analyses in Kelly and Wierzbicki (1967), Kelly and Wilshaw (1968), Calder and Goldsmith (1971) and Calder *et al.* (1971) were either bending only or membrane only, and no local indentations due to the striker were considered. Recently, some experimental tests have been carried out at the Impact Research Centre at the University of Liverpool to investigate the dynamic plastic response of thin circular plates struck transversely by a dropping mass with a conical head and a spherical nose at the centre of the plates. It has been observed that both local indentation and global deformation are significant and that neither bending moment nor membrane force can be neglected.

An approximate theoretical analysis for the dynamic plastic responses of thin circular plates struck transversely by a mass with a conical head and a spherical nose at the centre of the plates is presented in the next section. This analysis employs an interaction yield surface which combines the bending moment and membrane force required for plastic flow as in Jones (1971). Material strain rate sensitive effects are examined with the aid of the Cowper–Symonds equation (1957) and Perrone and Bhadra's approximation (1984). The numerical results for the maximum permanent deflection without failure are compared with the corresponding experimental data in Section 3, together with some observations, critical comments and discussions.

2. THEORETICAL ANALYSIS FOR A CIRCULAR PLATE UNDER IMPACT LOADING

The fully clamped circular plate in Fig. 1 has radius R, thickness H and mass density ρ, and is struck by a mass G travelling with an initial velocity V_0 at the centre of the plate. After impact, the striker G is assumed to remain in contact with the beam. Therefore, the striker and the struck point of the beam have an initial velocity V_0 at the instant of contact and a common velocity throughout the entire response.

The theoretical predictions in this article will be developed from a kinematically admissible viewpoint so that the static admissibility of the solution will not be examined for the assumed velocity profiles of the plate.

The maximum total deformation W_t is divided into two parts: maximum local indentation W_i and maximum global deflection W. A quasi-static method is used to analyse the local deformation, while the global deflection is studied with a dynamic analysis. Two values of the maximum local indentation W_i and the maximum global displacement W correspond to a common force magnitude between the striker and the impact point of the plate throughout the whole response.

Plastic yielding is controlled independently by the following two interaction yield conditions:

$$N_r^{*2} + M_r^* = 1 \tag{1}$$

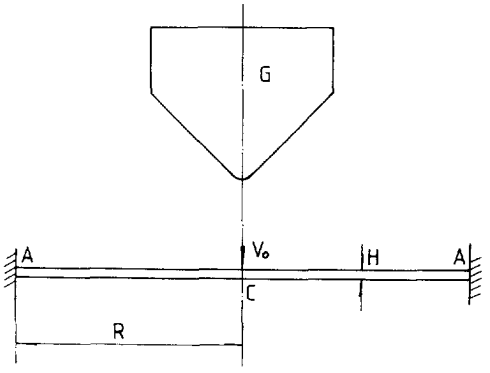

Fig. 1. A fully clamped circular plate struck transversely by a mass at the central point of the plate.

and

$$N_\theta^{*2} + M_\theta^* = 1, \tag{2}$$

where $M_r^* = M_r/M_{do}$, $M_\theta^* = M_\theta/M_{do}$, $N_r^* = N_r/N_{do}$, $N_\theta^* = N_\theta/N_{do}$, $M_{do} = \sigma_{do}H^2/4$ and $N_{do} = \sigma_{do}H$. The dynamic flow stress σ_{do} for a rigid, perfectly plastic material is taken as

$$\sigma_{do} = K\sigma_o, \tag{3a}$$

where

$$K = 1 + \left(\frac{\dot{\varepsilon}_m}{D}\right)^{1/p}, \tag{3b}$$

according to the Cowper–Symonds constitutive equation, where σ_o is the initial flow stress in a static uniaxial tensile test, D and p are material constants. The mean uniaxial strain rate $\dot{\varepsilon}_m$ in eqn (3b) is estimated by means of Perrone and Bhadra's approximation, which is further simplified by Jones (1989) as follows:

$$\dot{\varepsilon}_m = \frac{W_f V}{3\sqrt{2}L^2},$$

where L is the half length of the beam. For a circular plate, the above equation may be modified to

$$\dot{\varepsilon}_m = \frac{W_f V}{3\sqrt{2}R^2}, \tag{4}$$

where V in eqn (4) is part of the initial velocity V_o of the striker which produces only the global deformation of the plate and is calculated from the following equation:

$$\frac{GV^2}{2} = \frac{GV_o^2}{2} - E_{if}, \tag{5}$$

where E_{if} denotes the plastic work due to permanent local indentation, which will be deduced in the next section.

2.1. *Local indentation*

The indentation of the plate under the striker is observed to have the same shape as the head of the striker. It is assumed that any point x in the undeformed plate moves vertically to the point x' in the deformed plate, as shown in Fig. 2, so that

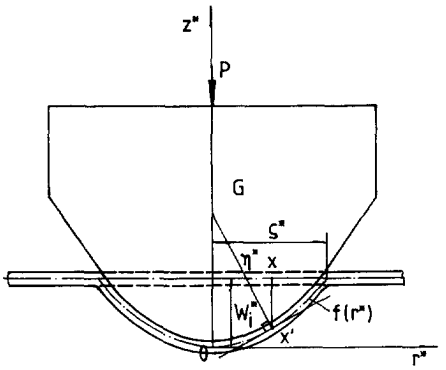

Fig. 2. Local indentation of the plate.

$$N_\theta = 0 \tag{6}$$

and

$$M_\theta = 1, \tag{7}$$

according to the normality of plasticity. The axisymmetric indented plate is formed by rotating the curve

$$z^* = f(r^*) \tag{8}$$

with regard to the axis, where $z^* = z/H$ and $r^* = r/H$.

The generalized radial membrane and bending strains are expressed as

$$\varepsilon_r = \sqrt{1+f'^2} - 1 \tag{9}$$

and

$$\kappa_r = |f''|/[(1+f'^2)^{3/2}H], \tag{10}$$

respectively, where $f' = \mathrm{d}f/\mathrm{d}r^*$ and $f'' = \mathrm{d}^2f/\mathrm{d}r^{*2}$. The radius of curvature in the θ direction in Fig. 2 is

$$\eta^* = r^*\sqrt{1+1/f'^2},$$

where $\eta^* = \eta/H$. The generalized circumferential bending strain is given as

$$\kappa_\theta = 1/\eta = 1/[r\sqrt{1+1/f'^2}]. \tag{11}$$

The normality rule applied to eqn (1) requires

$$\frac{\varepsilon_r}{\kappa_r} = -\frac{\mathrm{d}M_r}{\mathrm{d}N_r} = HN_r^*/2.$$

Let

$$\lambda = \frac{2}{H}\frac{\varepsilon_r}{\kappa_r}; \tag{12}$$

then

$$N_r^* = 2(\sqrt{1+f'^2} - 1)(1+f'^2)^{3/2}/|f''|, \tag{13a}$$

$$M_r^* = 1 - N_r^{*2}, \quad \text{if } \lambda < 1 \tag{14a}$$

and

$$N_r^* = 1, \tag{13b}$$

$$M_r^* = 0, \quad \text{if } \lambda \geqslant 1 \tag{14b}$$

when using eqns (9), (10) and (1).

The principle of virtual work requires that

$$P\,\mathrm{d}W_i = 2\pi(M_r\kappa_r + M_\theta\kappa_\theta + N_r\varepsilon_r)\zeta\,\mathrm{d}\zeta. \tag{15}$$

The plastic work due to the circumferential hinge at ζ which travels from ζ to $\zeta+\mathrm{d}\zeta$ is omitted in eqn (15). This is because $\lambda \gg 1$ from eqns (9), (10) and (12) except for small ζ, which results in $M_r = 0$. Hence, eqn (15) provides a satisfactory estimate. When taking $\mathrm{d}W_i = f'\,\mathrm{d}\zeta$ into account and using eqns (7) and (9)–(11), eqn (15) is recast as

$$P^* = [4N_r^*(\sqrt{1+f'^2}-1) + M_r^*|f''|/(1+f'^2)^{3/2}]\zeta^*/f' + 1/\sqrt{1+f'^2}, \tag{16}$$

where $P^* = P/(2\pi M_{do})$, N_r^* and M_r^* are determined with eqns (13)–(14), f' and f'' are functions of ζ and $\zeta^* = \zeta/H$. Thus, the relationship between P and W_i can be easily found from eqn (16) due to $W_i = f(\zeta)$.

The maximum permanent local indentation W_{if} corresponds to the moment when motion ceases. Thus, the plastic work due to the local indentation is

$$E_i = \int_0^{W_i} P\,\mathrm{d}z = \frac{\pi H^3\sigma_{do}}{2}\int_0^{\zeta^*} P^* f'\,\mathrm{d}\zeta^* \tag{17}$$

and the plastic work which corresponds to W_{if} is

$$E_{if} = \int_0^{W_{if}} P\,\mathrm{d}z = \frac{\pi H^3\sigma_{do}}{2}\int_0^{\zeta_f^*} P^* f'\,\mathrm{d}\zeta^*. \tag{17}'$$

2.2. *Global deflection*

The following two simplifications are introduced into the analysis by Shen and Jones (1993):

(a) The radial and circumferential membrane forces N_r and N_θ are equal (N) and are independent of the radial coordinate r.†

(b) Plastic yielding is controlled independently by eqns (1) and (2).

In view of assumption (a) the normality requirement of plasticity associated with M_θ^* and N_θ^* is disregarded.

2.2.1. *Phase* 1 : $0 \leqslant t \leqslant t_1$. The circular plastic hinge B starts to move from the centre C of the plate towards the support A in Fig. 3(a) when struck by a mass at $t = 0$, so that the transverse velocity field is now

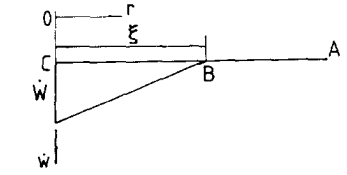

(a)

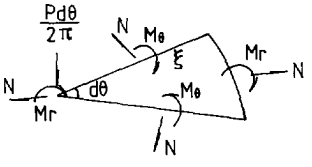

(b)

Fig. 3. Phase 1. (a) Velocity profile; (b) generalized forces and moments.

† This assumption is not valid for the corresponding infinitesimal displacement problem, but it does capture the main characteristics for a dynamic finite displacement problem which is dominated by membrane forces.

$$\dot{w} = \dot{W}(1-r/\xi), \quad 0 \leqslant r \leqslant \xi \tag{18a}$$

and

$$\dot{w} = 0, \quad \xi \leqslant r \leqslant R. \tag{18b}$$

Equilibrium of the fan-shaped elements in Fig. 3(b) with assumption (a) and equilibrium of the striker requires

$$\frac{\mathrm{d}}{\mathrm{d}t}\left[\int_0^{\xi} \rho H\dot{W}(1-r/\xi)r\,\mathrm{d}r\,\mathrm{d}\theta\right] = \frac{P}{2\pi}\mathrm{d}\theta, \tag{19}$$

$$\frac{\mathrm{d}}{\mathrm{d}t}\left[\int_0^{\xi} \rho H\dot{W}(1-r/\xi)r^2\,\mathrm{d}r\,\mathrm{d}\theta\right] = M_r\xi\,\mathrm{d}\theta + M_\theta\xi\,\mathrm{d}\theta + N\xi\,\mathrm{d}\theta W - N\xi\,\mathrm{d}\theta W/2 \tag{20}$$

and

$$P + G\ddot{W} = 0. \tag{21}$$

Equations (19)–(21) are recast as

$$\frac{\mathrm{d}}{\mathrm{d}t}(\dot{W}^*\xi^{*2}) = \frac{\beta}{2}P^*, \tag{19}'$$

$$\frac{\mathrm{d}}{\mathrm{d}t}(\dot{W}^*\xi^{*3}) = 2\beta\xi^*(M^* + N^*W^*) \tag{20}'$$

and

$$P^* + 6\delta/\beta\ddot{W}^* = 0, \tag{21}'$$

where $M_r = M_\theta = M$ due to assumption (a) and eqns (1) and (2), $\delta = G/(\rho\pi R^2 H)$, $\beta = 3\sigma_{\mathrm{do}}/(\rho R^2)$, $W^* = W/H$, $\xi^* = \xi/R$, $\dot{(\ )} = \partial(\ )/\partial t$ and $\ddot{(\ )} = \partial^2(\ )/\partial t^2$.

The yield condition now becomes

$$N^{*2} + M^* = 1. \tag{22}$$

The normality rule of plasticity demands

$$\frac{\dot{\Delta}/2}{\dot{W}/\xi} = -\frac{\mathrm{d}M}{\mathrm{d}N}$$

or

$$N^* = W^*, \quad W^* \leqslant 1 \tag{23a}$$

and

$$N^* = 1, \quad W^* > 1 \tag{23b}$$

when using eqn (22) and the approximate geometric relationship between the radial elongation and the displacement at the centre of the plate

$$\dot{\Delta} \cong W\dot{W}/\xi. \tag{24}$$

Equations (19)–(21)′ and (22)–(23) which contain five variables, W, ξ, M, N and P, give

$$\dot{W}^* = \frac{V_o^*}{1+\xi^{*2}/3\delta}, \tag{25}$$

$$\xi^* = \Gamma\frac{2\beta V_o^*}{\dot{W}^*(2\dot{W}^*+V_o^*)\xi^*}, \tag{26}$$

$$P^* = \Gamma\frac{8\dot{W}^*}{2\dot{W}^*+V_o^*} \tag{27}$$

and

$$W^* = \Psi, \quad W^* \leqslant 1, \tag{28a}$$

$$W^* = \sqrt{2\Psi-1}, \quad W^* > 1, \tag{28b}$$

where

$$\Psi = \frac{3\delta}{4\beta}(2V_o^{*2} - \dot{W}^{*2} - V_o^*\dot{W}^*), \tag{29}$$

$$\Gamma = 1, \quad W^* \leqslant 1, \tag{30a}$$

$$\Gamma = W^*, \quad W^* > 1 \tag{30b}$$

and $V_o^* = V_o/H$ when using the initial conditions $\dot{W}^* = V_o^*$, $W^* = 0$ and $\xi^* = 0$ at $t = 0$. This phase ends at $t = t_1$ when $\xi^* = 1$ and the associate velocity

$$\dot{W}_1^* = \frac{V_o^*}{1+1/3\delta} \tag{31}$$

and displacement

$$W_1^* = \Psi_1, \quad W_1^* \leqslant 1 \tag{32a}$$

and

$$W_1^* = \sqrt{2\Psi_1-1}, \quad W_1^* > 1, \tag{32b}$$

where

$$\Psi_1 = \frac{3\delta(2+9\delta)}{4\beta(1+3\delta)^2}V_o^{*2}, \tag{33}$$

will become the initial conditions of the next phase.

2.2.2. *Phase* $2: t_1 \leqslant t \leqslant t_f$ *stationary plastic hinge phase*. The transverse velocity profile for this phase of motion is

$$\dot{w} = \dot{W}(1-r/R), \quad 0 \leqslant r \leqslant R, \tag{34}$$

as shown in Fig. 4(a).

Equilibrium of the fan-shaped element in Fig. 4(b) and equilibrium of the striker requires

$$\frac{\mathrm{d}}{\mathrm{d}t}\left[\int_0^R \rho H\dot{W}(1-r/R)r\,\mathrm{d}r\,\mathrm{d}\theta\right] = \frac{P}{2\pi}\mathrm{d}\theta - QR\,\mathrm{d}\theta, \tag{35}$$

$$\frac{\mathrm{d}}{\mathrm{d}t}\left[\int_0^R \rho H\dot{W}(1-r/R)r^2\,\mathrm{d}r\,\mathrm{d}\theta\right] = M_r R\,\mathrm{d}\theta + M_\theta R\,\mathrm{d}\theta + NR\,\mathrm{d}\theta W - NR\,\mathrm{d}\theta W/2 - QR\,\mathrm{d}\theta R \tag{36}$$

and eqn (21), which are recast as

$$\dot{W}^* = \frac{\beta}{2}P^* - \frac{2\beta R}{\sqrt{3}H}Q^*, \tag{35}'$$

$$\ddot{W}^* = 2\beta\left(M^* + N^*W^* - \frac{2R}{\sqrt{3}H}Q^*\right) \tag{36}'$$

and eqn (21)′, where $M_r = M_\theta = M$ due to assumption (a) and eqns (1) and (2), $Q^* = Q/Q_{do}$ and $Q_{do} = \sigma_o H/\sqrt{3}$.

The normality rule of plasticity demands

$$\frac{\dot{\Delta}/2}{\dot{W}/R} = -\frac{\mathrm{d}M}{\mathrm{d}N}$$

or eqn (23) when using eqn (22) and the approximate geometric relationship between the radial elongation and the displacement at the centre of the plate

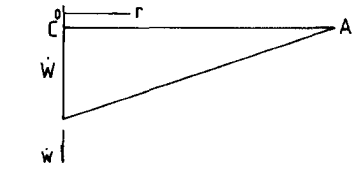

(a)

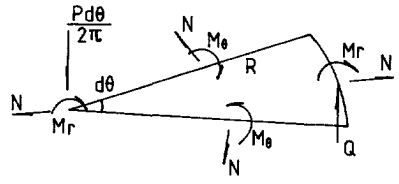

(b)

Fig. 4. Phase 2. (a) Velocity profile; (b) generalized forces and moments.

$$\dot{\Delta} \cong W\dot{W}/R. \tag{37}$$

Equations (21)′, (22) and (35)–(36)′, which retain four variables W, M, N and Q, yield the force–displacement relationship and the maximum displacement

$$P^* = \Gamma \frac{12\delta}{1+6\delta} \tag{38}$$

$$W_f^* = W_1^* + \frac{1+6\delta}{4\beta}\dot{W}_1^{*2}, \quad W_1^* \leqslant 1 \quad \text{and} \quad W_f^* \leqslant 1 \tag{39a}$$

$$W_f^* = \sqrt{\frac{1+6\delta}{2\beta}\dot{W}_1^{*2} + W_1^{*} - 1}, \quad W_1^* \leqslant 1 \quad \text{and} \quad W_f^* > 1 \tag{39b}$$

$$W_f^* = \sqrt{\frac{1+6\delta}{2\beta}\dot{W}_1^{*2} + W_1^{*2}}, \quad W_1^* > 1 \quad \text{and} \quad W_f^* > 1. \tag{39c}$$

The maximum permanent total deflection W_{tf} is the sum of W_{if} and W_f.

3. EXPERIMENTAL RESULTS AND THEORETICAL PREDICTIONS

Some experimental tests on circular plates struck transversely by a mass with a conical head and a spherical nose at the centre of the plates were carried out in the Impact Research Centre at the University of Liverpool. The circular plates of 6.2 mm thickness and 152.5 mm diameter ($H/2R = 0.0204$) were made of mild steel with a yield stress of 289 MN m^{-2} and were fully clamped.

The 76.5 kg indenter is shown in Fig. 5, having a conical head with a vertex angle of 90° and a spherical nose with a radius of 8 mm. The function $f(r^*)$ in eqn (8) for the indenter shown in Fig. 5 becomes

$$z^* = f(\zeta^*) = \begin{cases} a^* - \sqrt{a^{*2} - \zeta^{*2}}, & \zeta^* \leqslant a^*/\sqrt{2}, \\ \zeta^* + (1-\sqrt{2})a^*, & \zeta^* > a^*/\sqrt{2}. \end{cases} \tag{40}$$

Differentiating function f once and twice yields

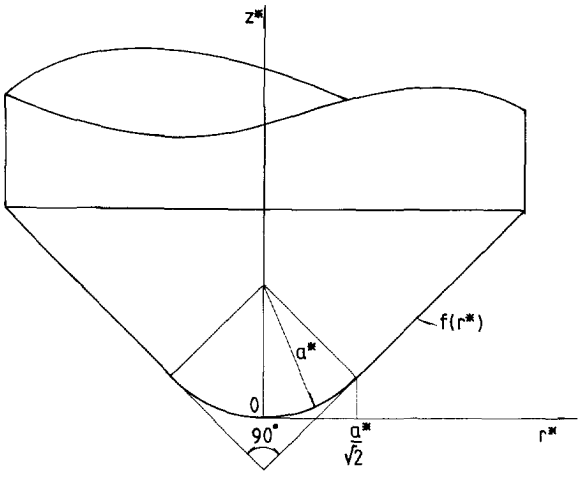

Fig. 5. Indenter having a conical head and a spherical nose.

$$f'(\zeta^*) = \begin{cases} \zeta^*/\sqrt{a^{*2}-\zeta^{*2}}, & \zeta^* \leqslant a^*/\sqrt{2}, \\ 1, & \zeta^* > a^*/\sqrt{2} \end{cases} \tag{41}$$

and

$$f''(\zeta^*) = \begin{cases} a^{*2}/(a^{*2}-\zeta^{*2})^{3/2}, & \zeta^* \leqslant a^*/\sqrt{2}, \\ 0, & \zeta^* > a^*/\sqrt{2}. \end{cases} \tag{42}$$

Thus, P^* and E_i can be found from eqns (16), (17), (41) and (42) as

$$P^*(\zeta^*) = \begin{cases} \sqrt{a^{*2}-\zeta^{*2}}\left[\dfrac{2}{a^*}+4a^*\left(\dfrac{a^*}{\sqrt{a^{*2}-\zeta^{*2}}}-1\right)^2\right], & \zeta^* \leqslant \zeta_o^*, \\ \sqrt{a^{*2}-\zeta^{*2}}\left[\dfrac{1}{a^*}+4\left(\dfrac{a^*}{\sqrt{a^{*2}-\zeta^{*2}}}-1\right)\right], & \zeta_o^* < \zeta^* \leqslant a^*/\sqrt{2}, \\ \dfrac{1}{\sqrt{2}}+4(\sqrt{2}-1)\zeta^*, & \zeta^* > a^*/\sqrt{2}, \end{cases} \tag{43a–c}$$

where

$$\zeta_o^* = a^*\sqrt{1-1/\left(1+\frac{1}{2a^*}\right)^2}$$

and

$$E_i(\zeta^*) = \begin{cases} F_1(\zeta^*)-F_1(0), & \zeta^* \leqslant \zeta_o^*, \\ F_2(\zeta^*)-F_2(\zeta_o^*)+F_1(\zeta_o^*)-F_1(0), & \zeta_o^* < \zeta^* \leqslant a^*/\sqrt{2}, \\ F_3(\zeta^*)-F_3\left(\dfrac{a^*}{\sqrt{2}}\right)+F_2\left(\dfrac{a^*}{\sqrt{2}}\right)-F_2(\zeta_o^*)+F_1(\zeta_o^*)-F_1(0), & \zeta^* > a^*/\sqrt{2}, \end{cases} \tag{44a–c}$$

where

$$F_1(\zeta^*) = \frac{\pi H^3\sigma_{do}}{2}\left[\left(\frac{1}{a^*}+2a^*\right)\zeta^{*2}-2a^{*3}\ln(a^{*2}-\zeta^{*2})+8a^{*2}\sqrt{a^{*2}-\zeta^{*2}}\right], \tag{45a}$$

$$F_2(\zeta^*) = \frac{\pi H^3\sigma_{do}}{2}\left[\left(\frac{1}{2a^*}-2\right)\zeta^{*2}-4a^*\sqrt{a^{*2}-\zeta^{*2}}\right] \tag{45b}$$

and

$$F_3(\zeta^*) = \frac{\pi H^3\sigma_{do}}{2}\left[\frac{1}{\sqrt{2}}\zeta^*+2(\sqrt{2}-1)\zeta^{*2}\right]. \tag{45c}$$

The maximum impact force and the maximum local plastic work are $P^*_{max} = P^*(\zeta_f^*)$ and $E_{if} = E_i(\zeta_f^*)$, respectively.

It is obvious that a in eqns (40)–(45) is $8+6.2/2 = 11.1$ mm for the specimens. D and p in eqn (3b) are 40 and 5, respectively, for the mild steel material.

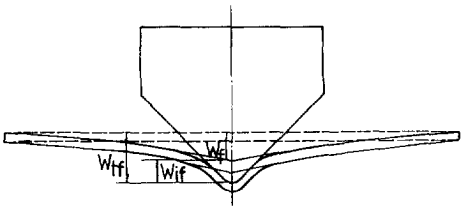

Fig. 6. Final deformation of the mild steel plate with $R = 152.5$ mm, $H = 6.2$ mm, $D = 40$, $p = 5$, $\rho = 7860$ kg m^{-3} and $\sigma_0 = 289$ MN m^{-2} struck transversely by a mass with $G = 75$ kg, $a = 8$ mm and $V_0 = 8.86$ m s^{-1}. (——) Total deformation with $W_{tf} = 32.69$ mm, (——) global deformation with $W_f = 18.17$ mm, (– – –) undeformed plate.

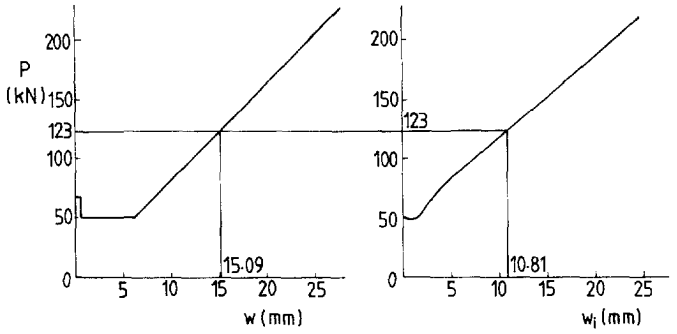

Fig. 7. Variations of the impact force P with global deflection W and local indentation W_i for the plate as in Fig. 6 except that $V_0 = 7.25$ m s^{-1}.

The dark solid lines in Fig. 6 show the permanent total deformation of the plate for an input kinetic energy of 3 kJ according to the present theoretical calculation. The maximum permanent total deflection W_{tf} of 32.69 mm consists of the maximum permanent global deflection W_f of 18.17 mm and the maximum permanent local indentation W_{if} of 14.52 mm. The dotted lines in Fig. 6 show the shape of the undeformed plate and the light solid lines denote the global deformation of the plate without local indentation. The ratios W_{if}/W_{tf} and W_f/W_{tf} are 44.4% and 55.6%. It transpires that the local indentation plays an important role in the total response of the plate and cannot be neglected.

The impact force P between the striker and the plate varies with the global deflection W and the local indentation W_i, as shown in Fig. 7 for an input kinetic energy of 2.01 kJ and a relative dynamic strengthening factor K of 1.46 from the calculated results. The maximum force is 123 kN, which corresponds to W_f and W_{if} of 15.09 mm and 10.81 mm, respectively. Figure 7 also reveals that the initial global deflection before reaching the pure membrane state is significant compared with the total global deflection and the initial local indentation.

Good agreement between the theoretical predictions and the experimental results were obtained for both the maximum permanent total deflections and the maximum force between the striker and the plates for an input energy ranging from 1 to 3.5 kJ, as shown in Figs 8 and 9, respectively.

However, more experimental results are required for the validation of the theoretical method. Furthermore, it would be interesting to extend the theory further using the energy density failure criterion of Shen and Jones (1992), to investigate the petalling failure of thin circular plates struck by non-blunt masses. This will be carried out in due course at the University of Portsmouth.

4. CONCLUSIONS

The approximate theoretical method presented in this paper provides an effective procedure for predicting the dynamic responses of circular visco-plastic plates struck transversely by a non-blunt heavy mass. Both bending moment and membrane force were considered in the plastic yielding. Strain rate sensitivity effects have been taken into account with the aid of the Cowper–Symonds equation and Perrone and Bhadra's approximation.

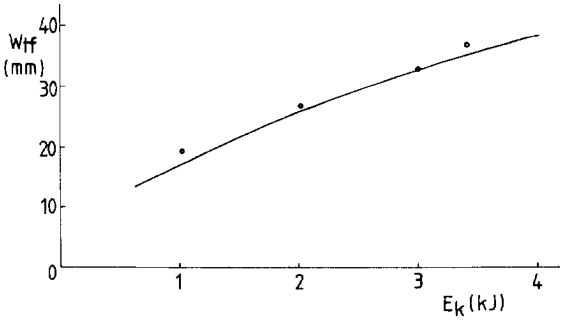

Fig. 8. Variation of the maximum permanent total deflection W_{tf} with input kinetic energy E_k for the plate as in Fig. 6. (•) Experimental results, (——) present theoretical predictions.

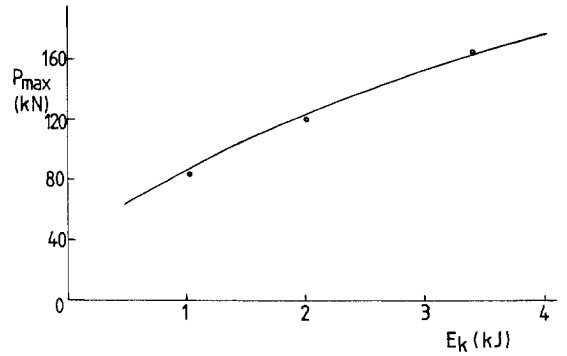

Fig. 9. Variation in maximum impact force P_{max} with input kinetic energy E_k for the plate as in Fig 6. (•) Experimental results, (——) present theoretical predictions.

Local indentation was considered, besides the global deformation, and was found to be significant. A striker with a conical head and spherical nose was used for the experimental tests. The formulae in Section 2 may be used for strikers of other shapes.

REFERENCES

Calder, C. A. and Goldsmith, W. (1971). Plastic deformation and perforation of thin plates resulting from projectile impact. *Int. J. Solids Structures* **7**, 863–881.

Calder, C. A., Kelly, J. M. and Goldsmith, W. (1971). Projectile impact on an infinite, viscoplastic plate. *Int. J. Solids Structures* **7**, 1143–1152.

Cowper, G. R. and Symonds, P. S. (1957). Strain hardening and strain rate effects in the impact loading of cantilever beams. Technical Report No. 28 from Brown University, Providence, to the Office of Naval Research under Contract No. 562(10).

Goldsmith, W., Liu, T. W. and Chulay, S. (1965). Plate impact and perforation by projectiles. *Experimental Mechanics*, 385–404.

Hopkins, H. G. (1953). On the impact loading of circular plates made of ductile metal. Division of Applied Mechanics, Brown University, Providence. Brown University Report No DA-2598/7, AD 22938.

Jones, N. (1971). A theoretical study of the dynamic plastic behaviour of beams and plates with finite-deflections. *Int. J. Solids Structures* **7**, 1007–1029.

Jones, N. (1989). *Structural Impact*. Cambridge University Press, Cambridge.

Kelly, J. M. and Wierzbicki, T. (1967). Motion of a circular viscoplastic plate subject to projectile impact. *Z. Angew. Math. Phys.* **18**, 236–246.

Kelly, J. M. and Wilshaw, T. (1968). A theoretical and experimental study of projectile impact on clamped circular plates. *Proc. Roy. Soc.* **A306**, 435–447.

Perrone, N. and Bhadra, P. (1984). Simplified large deflection mode solutions for impulsively loaded, viscoplastic, circular membranes. *J. Appl. Mech.* **51**, 505–509.

Recht, R. F. and Ipson, T. W. (1963). Ballistic perforation dynamics. *J. Appl. Mech.* **30**, 384–390.

Shen, W. Q. and Jones, N. (1992). A failure criterion for beams under impulsive loading. *Int. J. Impact Engng* **12**(1), 101–121.

Shen, W. Q. and Jones, N. (1993). Dynamic response and failure of fully clamped viscoplastic circular plates under impulsive loading. *Int. J. Impact Engng* **13**(2), 259–278.